

# Reliability Evaluation of IEEE 802.11p Broadcast Ad Hoc Networks on the Highway

Zhijuan Li, Yanbin Wang, and Jing Zhao

**Abstract**—In a vehicular ad hoc network (VANET) based on IEEE 802.11p, the performance of the communication link is heavily influenced by interference. To quantify the impact of interference, analytical models usually explicitly or implicitly assumed the interference range beyond which interference is ignored. We find that the potential maximum interference range should be related to the minimum interference power that the device can perceive. However, most previous works on VANET performance modeling simply assumed a fixed interference range. The most recently proposed effective interference range dependent on the signal-to-interference-and-noise ratio (SINR) threshold may appear to exceed the potential maximum interference range, resulting in an overestimation of the impact of interference. This paper proposes the SINR related Effective Distance Constrained by the Maximum interference range-based (SED-CM) model for IEEE 802.11p VANET performance evaluation on the Highway. First, we give the potential maximum interference range setting by studying the empirical distribution of interference distance corresponding to the minimum interference power in NS2 simulation. The performance metrics are then derived. The proposed SED-CM model is further extended to the intersection scenario. We conducted extensive NS2 simulations to evaluate the proposed model and compare it with three typical models. Results show that the SED-CM model presents the best evaluation ability. Moreover, we experimentally analyzed the effect of vehicle speed on the performance of VANET by mapping the vehicle speed to the vehicle density. Results show that a faster beacon rate is required to meet the reliability requirement of safety applications with the increase in vehicle speed.

**Index Terms**—IEEE 802.11p, Signal-to-interference-and-noise ratio, Reliability, Dedicated short-range communication

## I. INTRODUCTION

### A. Motivation

Vehicular ad hoc network (VANET) is the underlying communication technology to provide many safety services for intelligent transportation systems (ITS) [1]. In 2010, the IEEE published the wireless access in vehicular environment (WAVE) amendment to enable direct and short-range communications (DSRC) between vehicles [2]. The amendment was formally standardized as IEEE 802.11p, which defined many communication parameters that can be adjusted within

a limited range separately or in combination [3], [4] to ensure the high quality of service (QoS) and low latency requirements of safety services in different environments. For example, beacon messages are generated periodically, and the generation rate  $\lambda$  is defined 10 Hz [3] in IEEE 802.11p, which can not always meet the reliability requirement. Eight data rates  $R_d$  corresponding to the adopted modulation and coding schemes (MCSs) vary from 3 Mbps to 27 Mbps, and they could be switched by setting the available transmit power in the physical (PHY) layer [5]. Carrier sensing threshold controls the carrier sensing range, which could be set in the PHY/MAC layers to any value [6] to achieve the target demand for throughput or reliability of the system. These parameters together affect the performance of the network and their adaptation and trade-off are critical issues. It is expected that the communication parameters, impact factors and traffic environments, etc., in the real-world system are accurately fed to QoS analytical model. Then VANET could adapt these parameters relying on the immediate predict capacity of the analytical models.

IEEE 802.11p defines carrier sense multiple access with collision avoidance (CSMA/CA) as the basic channel access mechanism. The CSMA/CA without "Request To Send/Clear To Send (RTS/CTS)" [7] is used for broadcast communication of VANET. In this way, interference heavily influenced the performance of VANET. Due to CSMA, the concurrent transmissions within the sensing range and the hidden terminals beyond the sensing range are two types of interference that reduce the signal-to-interference-and-noise ratio (SINR). The concurrent transmissions could cause interference if the backoff counter is zero as the backoff counter of the tagged sender simultaneously. The hidden terminals could cause interference since CSMA has no effective collision avoidance mechanism to deal with. The interference occurs when the transmission of hidden terminals overlaps with the transmission of the intended sender in part or whole. The interference probability in the case relates closely with the length of packet transmission time, which is different from the concurrent collision in that the backoff counters reach zero. Moreover, the interference analysis encounters the minor modeling uncertainties [8] since reference changes over time under the impact of the CSMA, the imperfect channel, and the changing traffic environments.

Various models for IEEE 802.11p VANET performance evaluation have been constructed by applying stochastic geometry or probability modeling to the interference analysis. We classify these analytical models into four types, the Deterministic Distance-based (DD) model, the SINR Probability Derivation-based (SPD) model, the SINR related Effective Distance-based (SED) model, and the stochastic geometry-

Copyright (c) 2015 IEEE. Personal use of this material is permitted. However, permission to use this material for any other purposes must be obtained from the IEEE by sending a request to pubs-permissions@ieee.org.

Zhijuan Li and Yanbin Wang are co-first authors. Corresponding author: Jing Zhao

Zhijuan Li is with the College of Computer Science and Technology, Harbin Engineering University, Harbin, 150001, China (e-mail: lizhijuan@hrbeu.edu.cn).

Yanbin Wang is with the Department of Industrial Engineering, Harbin Institute of Technology, Harbin, 150001, China (e-mail: wangyb@hit.edu.cn).

Jing Zhao is with School of Software, Dalian University of Technology, Dalian, 116024, China (e-mail: zhaoj9988@dlut.edu.cn).

based model. As the signal attenuates with distance, there is a key issue on how far interference should be incorporated into the analytical model. These existing models explicitly or implicitly assumed the interference range beyond which interference is ignored. The DD model [9], [10] assumed the interference range equals the sensing range, irrespective of the location of the receiver. The SPD [11], [12] model took the interference within twice the sensing range of the intended transmitter into account, the interference range is approximately equal to the sensing range. The typical stochastic geometry-based model [13] evaluated the transmission success probability using an evaluator based on Matérn Hard-core process. The interference range does not exceed the size (length) of the simulation scene. The recently proposed SED model [2], [14] adopted the effective interference range depending on the SINR threshold. These researches will be explained in further detail in Section I-B related work. The signal is the actual interference if its power is greater than or equal to the minimum interference power that the device can perceive depending on specific hardware features [15], [16]. The minimum interference power reveals the potential maximum interference range. However, the above interference range assumptions did not consider the maximum interference range leading to overestimating the impact of interference or underestimating the effect.

How to determine the maximum interference range is an important problem to be solved. We research the setting of the maximum interference range, the impact of the maximum interference range and focus on improving the accuracy of the analysis model in the one-dimensional (1D) Highway and two-dimensional (2D) intersection scenarios. [17] has verified that the NS2 simulator could accurately model the MAC and PHY associated with an IEEE 802.11 hardware implementation. In this way, it is feasible to use simulation as the primary investigative tool. We determine the setting of maximum interference range by obtaining the distribution of interference distance in NS2, and propose the SINR related Effective Distance Constrained by the Maximum interference range-based (SED-CM) analytical model. The proposed model is the extension of the SED analytical model [14], general and efficient. Then we extend the SED-CM model of the 1D Highway to a 2D intersection scenario by combining more interference areas. In addition, we comprehensively study the effect of vehicle speed on the performance of the system by mapping the vehicle speed to vehicle density, exploring and facilitating the provision of optimization schemes.

## B. Related work

The analytical models play an important role in the optimization and congestion control scheme since they provide timely QoS metrics for comparison. For example, [18] developed an optimization scheme to find optimal beacon rates by a utility maximization framework which accounted for the reliability of safety messages and maintaining the accuracy of awareness. [3] proposed a joint adaptation scheme of the beacon rate and power, relying on an altruistic short-term prediction algorithm to estimate the vehicular density, enabling

a significant enhancement in terms of channel busy ratio and awareness among vehicles. [10] proposed a multi-object multi-parameter optimization scheme based on Bare Bones Particle Swarm Optimization (BBPSO) algorithm to maximize the transmission capacity and minimize the delay while satisfying the reliability requirement of safety application in dynamically changing environments. Moreover, the comparison work between DSRC and other protocols has been done based on their analysis. [5] theoretically analyzed IEEE 802.11p and LTE-V2V with resource allocations performed by the infrastructure, and comparison between analysis results showed that IEEE 802.11p has better performance at a short distance, but LTE-V2V has better capacity at a larger awareness range in a common scenario with consistent settings.

The DD models have been widely used to evaluate communication reliability of VANET and awareness capacity of safety applications in the 1D Highway [5], [9], [18]–[22], 2D intersection [23], and general  $d$ -dimensional ( $1 \leq d \leq 3$ ) scenes [10]. The model usually assumed that the interference range denoted by  $r_I^{\text{Fix}}$  is equal to the sensing range  $r_E$ , meaning that the mean minimum interference power equals the sensing threshold by the path loss law. The DD models assumed that an interferer within the interference range would deterministically make the reception fail, thus, they evaluated the impact of interference on reliability by calculating the interference probability of hidden terminals and concurrent transmissions. The models are efficient, but it is not feasible to apply the models in the changing network environments. On the one hand, the models may overestimate the effect of interference within the interference range assumption since the SINR distribution is not considered. On the other hand, the models may underestimate the interference due to ignoring the interference beyond  $r_I^{\text{Fix}}$ . It is difficult to determine the error trend between this model and the actual system.

Ni *et al.* [11], Ma *et al.* [24] and Zhao *et al.* [12] built the SPD model to derive the SINR distribution by assuming the log-normal or non-homogeneous poisson process (NHPP) vehicle distribution, CSMA mechanism, and Nakagami fading, and approximated the reliability metrics and link capacity based on the SINR distribution. These models took the transmission of the nodes within  $2r_E$  of the intended transmitter as the interference of receivers. Thus, for the receiver on the right of the sender which is the origin, the interference range on the left around the receiver denoted by  $r_I^{\text{Asy}-1}$  equals  $2r_E + d_S$ , where  $d_S$  is the distance between the sender and the receiver, and the interference range on the right around the receiver denoted by  $r_I^{\text{Asy}-2}$  equals  $2r_E - d_S$ . At the same time, the models accumulated the interference power to the interference only if the interference power was greater than or equal to the sensing threshold. In this way, the mean minimum interference power considered in the models is approximately equal to the sensing threshold. The models may underestimate the interference since they did not consider the interference beyond the interference range assumption. The models are not suitable for optimization of VANET since they are computationally intensive, involving multiple integrals and convolutions.

Stochastic geometry is a popular tool to characterize SINR

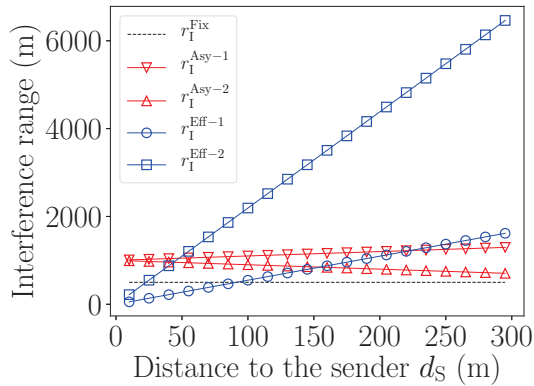


Fig. 1: The different interference range assumption,  $r_E = 500$  m,  $\theta = 14$  dB

and the related performance metrics of wireless networks, e.g., error probability [25], outage probability [25], coverage probability [26], [27], transmission rate [26], transmission success probability [28], packet loss probability [29], and so on. The interference protection of CSMA protocol brings difficulties to modeling CSMA and deriving closed-form expressions of performance metrics by stochastic geometry. [13] proposed an evaluator based on a hard-core process to count the transmission success probability of communication link, considering the interference protection of CSMA and the concurrent transmission within the sensing range. The model does not explicitly give the interference range assumption, which could be controlled by setting the minimum power for interference accumulation. However, the evaluator runs in a circle lane with a perimeter of 10000 m, meaning that the interference range can be up to and not exceed 10000 m. Although the interference range is much larger than the interference range assumption of the DD and SPD models, whether it is large enough is a question. In addition, two issues limit the application of this estimator. On the one hand, the parameters used in the evaluator rely on the statistical value in NS2. On the other hand, the model could not characterize the impact of the hidden terminal because it did not relate to packet transmission time precisely.

Recently, the SED model proposed in [2], [14] conducted SINR analysis of IEEE 802.11p VANET by converting the SINR distribution derivation to estimating the effective interference area depending on the SINR threshold, then derived reliability metrics and channel capacity. The SED model is more general and faster because it considered the SINR distribution and integrated the efficiency of the DD model. Two kinds of effective distance are given.  $r_I^{\text{Eff}-1}$  presents such effective interference distance within which the transmission of one node will deterministically make SINR less a given threshold  $\theta$ , resulting in the reception failure. The SINR is simplified to a signal-to-interference ratio (SIR) in the presence of interference. Then, we can calculate  $r_I^{\text{Eff}-1}$  by the path loss law and the definition of SIR, we have

$$\text{SIR} = \frac{P_t G_t G_r \eta \left(\frac{d_0}{d_s}\right)^\alpha}{P_t G_t G_r \eta \left(\frac{d_0}{d_I}\right)^\alpha} \leq \theta, \quad (1)$$

then,

$$d_I \leq \theta^{\frac{1}{\alpha}} d_s, \quad \text{and} \quad r_I^{\text{Eff}-1} = \theta^{\frac{1}{\alpha}} d_s \quad (2)$$

where  $P_t$  is the transmit power,  $G_t$  is the transmitter gain,  $G_r$  is the receiver gain,  $\eta = (c/4\pi d_0 f)^\alpha$  is a dimensionless constant in the path loss law determined by the carrier frequency  $f$  and the reference distance  $d_0$  for the antenna far field.  $c$  is the speed of light.  $\alpha$  is the path loss exponent, which is usually obtained by actual measurement. Generally,  $\alpha$  is 2 for free space environments, 1.6-1.8 for sight distance environments, and 2.7-5 for obstacle environments or urban areas.  $d_s$  is the receiving distance,  $d_I$  is the interference distance.  $r_I^{\text{Eff}-1}$  is the distance between the receiver and the farthest interferer whose transmission makes SIR equaling the SIR threshold. Another possible interference case making the SIR less than the threshold is that there is an interferer on the left and right sides of the sender, respectively. Similar to  $r_I^{\text{Eff}-1}$ ,  $r_I^{\text{Eff}-2}$  is the distance between the receiver and the farthest interferer in this case. We have the following inequality.

$$\text{SIR} = \frac{P_t G_t G_r \eta \left(\frac{d_0}{d_s}\right)^\alpha}{2P_t G_t G_r \eta \left(\frac{d_0}{d_I}\right)^\alpha} \leq \theta, \quad (3)$$

then

$$d_I \leq (2\theta)^{\frac{1}{\alpha}} d_s, \quad \text{and} \quad r_I^{\text{Eff}-2} = (2\theta)^{\frac{1}{\alpha}} d_s \quad (4)$$

Obviously,  $r_I^{\text{Eff}-2} > r_I^{\text{Eff}-1}$ .

(2) and (4) show that the effective interference ranges increase linearly with the receiving distance and the slope is greater with a larger SINR threshold. Fig. 1 presents the interference range assumptions of the DD, SPD, and SED models with the sensing range of 500 m and SINR threshold of 14 dB. Obviously, the effective interference range is slightly smaller than the sensing range at close range, but it quickly increases to be larger than the sensing range assumptions of DD and SPD models, and the gap is larger with a larger SINR threshold. Such a large effective interference range results in interference that is less than the device can detect may be included, thereby overestimating the impact of interference. It is more reasonable to limit the effective interference range to be smaller than the maximum interference range. Moreover, [14]'s experiment explicitly adopted 5000 m as an upper limit of  $r_I^{\text{Eff}-1}$  of SED model. In subsequent comparisons, we also adopted 5000 m as an upper limit of  $r_I^{\text{Eff}-1}$  of the SED model.

In summary, the model in this paper differs from our previous work in [12], which built the SPD model to derive the SINR distribution within the twice sensing ranges of the tagged sender. The model in [12] is time-cost because multiple integrals and convolutions are involved. Moreover, the model in the paper extends the research [14], of which we are co-authors. Both models derive performance metrics by estimating the effective interference area depending on the SINR threshold. Compared with [14], the effective interference area in the model does not increase infinitely and should be less than the potential maximum interference range, motivating a more precise interference analysis.

### C. Contributions

The main contributions of the paper are summarized as follows.

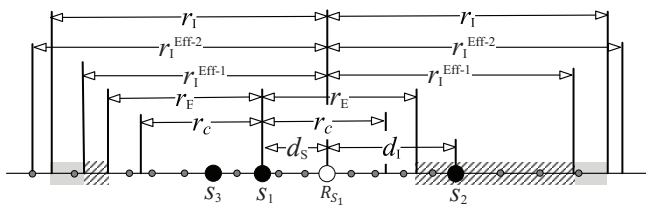


Fig. 2: General interference model for 802.11p VANET on the Highway

- 1) We obtain the interference distance distribution by NS2 simulation and give the maximum interference range setting of the analytical model for IEEE 802.11p VANET.
- 2) We propose the SINR related Effective Distance Constrained by Maximum interference range-based (SED-CM) model, which drives a more accurate evaluation on the impact of interference. The utility of the model is validated through the cross-validation experiments with NS2 simulation and the comparison experiments with previous models.
- 3) We extend the SED-CM model to the intersection scenario for performance evaluation. Compared with the 1D scenario, more interference areas are considered.
- 4) We conduct experiments to analyze the impact of speed on the performance of the network. The optimal beacon rates are witnessed at the given vehicle speed considering the awareness probability of safety applications and the channel busy ratio.

#### D. Organizations

The remainder of the paper is structured as follows. Section II presents problem formulation and describes the related background models on the packet reception procedure and channel fading in the PHY layer, as well as channel access mechanism in the MAC layer. Section III introduces the NS2 simulation settings, experimentally compares and discusses the stationary and mobility scenarios simulations as well as different PHY layer strategies, and provides the relationship between vehicle speed and density by fitting the data of SUMO and the Greenshields model. Section IV presents the interference distance distribution in NS2 and gives maximum interference range setting. Section V presents the proposed SED-CM model for IEEE 802.11p VANET performance evaluation in a 1D Highway scenario. The model is extended to the intersection scenario in Section VI. Section VII presents the experiment results. The paper is concluded in Section VIII.

## II. PROBLEM FORMULATION AND BACKGROUND MODEL

### A. Problem formulation

We consider the IEEE 802.11p VANET at 1D Highway. The interference model is abstracted as shown in Fig. 2. The horizontal straight line represents the Highway, and the dots on the line represent vehicles that periodically broadcast/receive basic safety messages (BSMs) to/from nearby vehicles. These messages are expected to be delivered with high quality and low latency to ensure upper-layer safety applications.

However, due to channel attenuation, channel access lacks central control, and there is no RTS/CTS mechanism, packet loss would occur and would be severe under inappropriate communication settings. In this way, based on the parameter settings and the vehicular environments, we construct the analytical model for VANET, which could derive MAC layer metrics point-to-point packet reception probability (PRP), packet reception ratio (PRR), channel busy ratio (CBR), and awareness probability (PA) of safety applications, paving the way to network planning and optimization.

As shown in Fig. 2,  $r_E$  and  $r_C$  denote the sensing range and communication range of the sender  $S_1$ , respectively, where  $r_C \leq r_E$  [12].  $d_S$  is the distance between the tagged sender  $S_1$  and the receiver  $R_{S_1}$ .  $S_2$  and  $S_3$  are the transmitters who send as  $S_1$  at the same time, thus, they are the interferer of  $S_1$ , interfering  $R_{S_1}$  receiving the packet of  $S_1$ .  $r_I$  is the potential maximum interference range around the receiver, which is determined by (5).

$$r_I = \min(d_0 \sqrt{P_t G_t G_r \eta / I_{th}}, I_{max}) \quad (5)$$

where  $I_{th}$  denotes the minimum interference power,  $I_{max}$  is such interference range after which the distribution of interference distance changes slightly. We will explain (5) in Section IV.  $d_I$  presents the interference distance between the receiver  $R_{S_1}$  and the interferer  $S_2$ .  $r_I^{EFF-1}$  is the farthest interference distance in which one interferer could make SINR less than the SINR threshold, calculated by (2).  $r_I^{EFF-2}$  is the farthest interference distance in which two interferers could make SINR less than SINR threshold, calculated by (4).

To facilitate analysis, we make the following assumptions. 1) All vehicles are treated as homogeneous with identical vehicle length  $L_V$  and the same communication parameters, e.g., transmission power  $P_t$ , data rate  $R_d$ , and so on. 2) All vehicles have equal sensing range  $r_E$ , communication range  $r_C$ , and interference range  $r_I$ . 3) We consider these vehicles following the homogeneous Poisson process (HPP) with the density  $\beta$ . 4) At each vehicle, the time interval between the arrival of two consecutive packets follows Exponential distribution with the rate  $\lambda$  (Hz). 5) The queue length of packets at each node is unlimited. In this way, each node can be modeled as a discrete-time Markov arrival/General service distribution/one service channel (M/G/1) queue [9]. 6) We adopt *Nakagami* fading model to evaluate the impact of the imperfect channel. 7) We do not consider the capture effect and successive interference cancellation (SIC) [30]. 8) We do not consider the impact of vehicle mobility on the performance of communication link in the MAC layer. On the one hand, the node is almost stationary within one packet transmission duration, which is usually less than 1 ms [13]. On the other hand, the measured packet loss rate (PLR) is not sensitive to Doppler spread at different vehicular speed settings [31]. Thus, the impact of mobility on the link can be neglected. 9) The vehicle speed acts on the tolerance time window for safety applications [32]. We will adopt the Greenshields model to represent the vehicle speed at the given density by assuming that the vehicle density is independent of the vehicle speed [33], [34]. Then the reliability of the safety application and the impact of speed on the safety application can be measured.

### B. Packet reception model

When multiple packets arrive at the receiver at the same time, for any one signal, the sum of all other ongoing signals is regarded as interference. Then the condition for a packet to be received is that the SINR is greater than the SINR threshold, and the received power is greater than the received power threshold.  $SINR = P_r / (S_I + N_0)$ , where  $P_r$  is the receiving power of the intended packet,  $S_I$  is the sum of the received power (i.e., interference power) of all arriving packets except the intended packet,  $N_0$  is the power of noise. Moreover, the processing mechanisms of different PHY layer strategies are also related to the order in which the packets arrive. The conventional PHY layer would drop all packets that arrived simultaneously if the reception of the first packet that arrived failed. Capture effect is such technology that when the first arriving packet fails to receive, the PHY layer will switch to receive the later arriving data packet with a better signal. SIC is advanced PHY layer technology proposed to combat interference for multi-packet reception [30]. In the model, the packets that meet the received power and SINR requirements can be received, regardless of the order in which the packets arrive. In Section III-E, we do experiments to compare the three PHY layer strategies and the analytical model while adopting the conventional CSMA as the MAC layer.

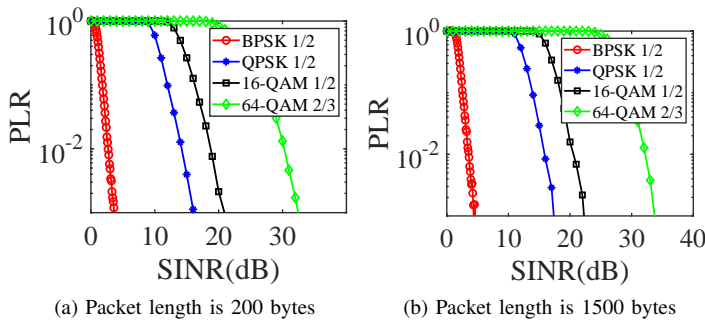


Fig. 3: PLR/SNR curves

In practice, the packet loss at instantaneous SINR is probabilistic in terms of the PLR/SINR curve. Fig. 3 shows PLR/SINR curves at different MCSs (Corresponding to different data rates [35]) when the packet length equals 200 bytes and 1500 bytes [36]. At the given SINR, PLR is calculated relying on the bit error ratio (BER) and the packet length PL.  $PLR = 1 - (1 - BER)^{8 \cdot PL}$ . Moreover, the general expressions between BER and SINR could be built by outdoor vehicular experiments or theoretical approximation [37]. Herein, we obtained BER/SINR curves by Matlab simulation. DSRC systems employ the Orthogonal Frequency Division Multiplexing (OFDM) technology in the PHY layer [38]. We use Matlab to implement an IEEE 802.11p PHY layer specifications compliant OFDM system to count BER at the given SINR. An OFDM symbol includes 48 data subcarriers and four pilot subcarriers in the simulation. FFT period is 6.4  $\mu$ s. The length of cyclic prefix (CP) is 16. The channel is Nakagami fading ( $m = 3$ ) plus additive white Gaussian noise (AWGN). Fig. 3 shows that the larger the SINR, the smaller the PLR. A certain acceptable PLR could determine

the SINR threshold. At the same time, we can find that PLR changes with the size of the packet and different MCSs. Specifically, based on the relationship between MCSs and data rates [35], we could find that the faster the data rate, the greater the SINR under the same PLR. The more the packet size, the greater the SINR under the same PLR. Then the SINR threshold corresponding to the acceptable PLR increases with the increase both in the packet size and the data rate. Without loss of generality, the analysis model with a feasible SINR threshold is necessary.

### C. Channel fading model

In this paper, we consider the imperfect channel using Nakagami fading model [39], [40]. The model was built based on the empirical results, which could better capture signal attenuation and path loss. Then, the power  $P_r$  and the average power  $\omega$  received of a receiver with distance  $d$  away from the transmitter are as follows:

$$\begin{aligned} P_r(d) &= \omega(d) \cdot G_f \\ \omega(d) &= P_t \cdot G_t \cdot G_r \cdot \eta \cdot l(d) \end{aligned} \quad (6)$$

where  $l(d)$  is the path loss between two communication nodes. It is modeled as  $l(d) = \min\{1, (\frac{d_0}{d})^\alpha\}$  and  $G_f$  is such random variable characterized by the probability density function (PDF)  $f(z)$ .

$$f(z) = \frac{m^m}{\Gamma(m)} z^{m-1} \exp(-mz) \quad (7)$$

where  $\Gamma(\cdot)$  is the standard Gamma function,  $m$  is the fading parameter in the given receiving distance. The sensing threshold is denoted by  $P_{th}$ . Then, the average sensing range  $r_E$  ( $r_E > d_0$ ) is the receiving distance with the average receiving power  $P_{th}$ , which can be expressed as follows.

$$r_E = d_0 \sqrt[m]{P_t G_t G_r \eta / P_{th}} \quad (8)$$

### D. Channel access model

In VANETs, each vehicle accesses the channel under the control of the CSMA/CA mechanism, achieving distributed coordinated access to the channel. Each node keeps a queue for packets to be sent. The nodes are in an idle state when their queues are empty. Newly generated packets enter the queue according to first-in, first-out (FIFO). When the first packet enters the queue, the node is awakened to monitor channel activity. If the channel is sensed free for a period equaling arbitration inter-frame space (AIFS), the node transmits and changes from an idle state to a transmission state. Otherwise, if the channel is sensed busy in AIFS time, the node starts a backoff counter with the initial value randomly selected in  $[0, 1, 2, \dots, W - 1]$ , where  $W$  is the size of the contention window. The node persists in monitoring the channel activity. If the channel is sensed free during a time slot of the backoff process, the backoff counter will be decreased by one. Otherwise, the backoff counter of the node will be frozen. Once the backoff counter reaches zero, the node transmits and enters a transmission state. After completing the transmission, the queue may or may not be empty. The node will change

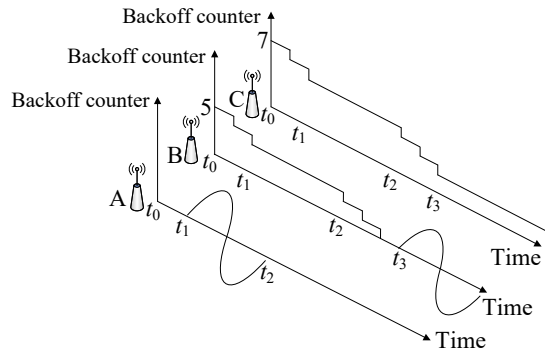


Fig. 4: Example of a backoff process formed by three nodes with packets to send

from transmission state to idle state if the queue is empty. Otherwise, the node will sense the channel again for AIFS time and then randomly choose a backoff counter to compete for the channel for the next packet. Fig. 4 shows an example of the backoff procedure formed by three nodes. Nodes A, B, and C are within the mutual sensing range. They have packets to send. At  $t_0$ , the backoff counter of A reaches zero, the backoff counter of C is bigger than the backoff counter of B. At  $t_1$ , A begins to transmit, the backoff counters of B and C are frozen, they are unfrozen after the packet of A has finished sending. In turn, at time  $t_3$ , B starts to transmit when its backoff counter reaches zero, and the backoff counter of C is frozen. Later, the backoff counter of C is unfrozen after the sending of B is finished. C would send directly once its backoff counter reaches zero.

### III. NS2 SIMULATION AND SPEED-DENSITY RELATIONSHIP FITTED BY SUMO

We adopt NS2 to analyze the distribution of the interference distance for determining the maximum interference range setting and validate the analytical model. Herein, we first present the critical parameter settings and describe the parameter to adjust the minimum interference power. Second, we compare PRPs and PRRs of the stationary and mobility scenarios simulations in NS2. The density in the stationary scenario is set to be the same as the mobility scenario driven by the trace of SUMO. Comparison results show that simulation in the stationary scenario is feasible. Then, we give the relationship between average vehicle speed and vehicle density by fitting the data from SUMO and the Greenshields model [41]. Furthermore, we compare the PRPs and PRRs of the network with the conventional CSMA together with different PHY layer strategies, including SIC, capture effect, and the conventional PHY layer reception strategy. The analysis results of the SED-CM model are also compared. The result shows that the difference is not obvious between our analysis model and capture or SIC enabled systems. In this way, the capture effect in NS2 is enabled in the cross-validation experiments.

#### A. Critical parameter settings

The interference models in NS2 have evolved in terms of complexity and sophistication [42]. Currently, the newest

TABLE I: Simulation parameters

Parameters	Values
Carrier frequency $f$	5.9 GHz
Channel bandwidth	10 MHz
Transmit power $P_t$	26 dBm
Average sensing range $r_E$	500 m
Carrier sensing threshold $P_{th}$	-76 dBm
Reference distance $d_0$	1 m
Noise floor power $N_0$	-95 dBm
Transmit gain $G_t$	1.0
Receive gain $G_r$	1.0
Constant $\eta$	1.64e-5
CW $W-1$	15
Path loss exponent $\alpha$	2
AIFS	58 $\mu$ s
Packet length PL	200 bytes
Slot time $\sigma$	13 $\mu$ s
Data rate $R_d$	24 Mbps
PHY preamble + header $T_{H1}$	40 $\mu$ s
MAC header $T_{H2}$	272 bits
PLCP header $T_{H3}$	4 $\mu$ s
Packet generation interval $T_c$	0.1 s
Fading parameter $m$	3, for $d_S \leq 50$ m 1.5, for $50 \text{ m} < d_S \leq 100$ m 1, for $d_S > 100$ m

NS2 version 2.35 integrated the wireless simulation modules revised by Chen *et al.* [35]. Chen's module adopted the additive interference model, which is more in line with the actual situation and has been widely used. At the same time, we have modified the module to enable the flexible SINRTs setting [12]. In the module, the variable  $CSThresh_$  presents the sensing threshold. When the signal power is below  $CSThresh_$ , the current channel is considered free. When a signal arrives, the method `recordPowerLevel()` is called to record the latest signal power of the current channel [43]. In `recordPowerLevel()`, the power of new arrival signal will be compared with  $PowerMonitorThresh_$ . If the signal power is greater than or equal to the  $PowerMonitorThresh_$ , the signal will be cumulated to the channel signal power, else it will be ignored. In this way, we can change the sensing range and the interference range by setting  $CSThresh_$  and  $PowerMonitorThresh_$  in the user-programmable Tcl script. The value of  $PowerMonitorThresh_$  refers to the minimum interference power, which could be determined by actual measurement. Table I lists the critical communication parameters.

#### B. Mobility scenes generated by SUMO

We adopt traffic simulation software SUMO to generate mobility traffic in a two-lane, two-way circular road. As shown in Fig. 5, the length of the lane is greater than 6000 m, the height is greater than 600 m, and the width of each lane is 3.2 m. We generate three groups of mobility traffic with different average vehicle speeds. Table II shows the mean speed, the maximum speed, and the minimum speed in the three groups of experiments. The acceleration is 2.9 m/s<sup>2</sup> (e.g., 2019 Volkswagen e-Golf SE [44]), the deceleration is

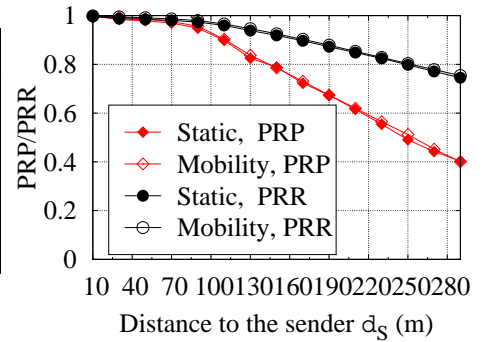
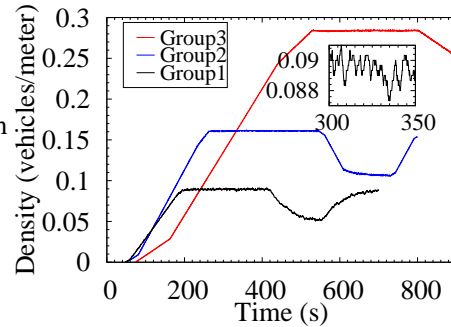
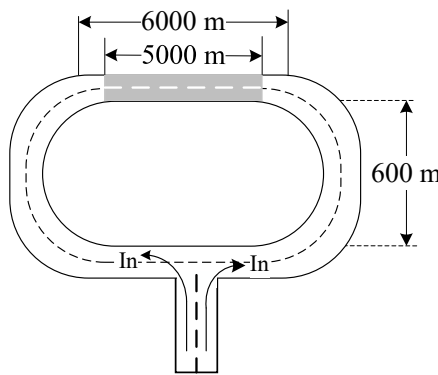


Fig. 5: Mobility traffic scenario generated by SUMO

Fig. 6: The changing density v.s. time

Fig. 7: PRP and PRR comparisons between stationary and mobility scenarios simulations

7.5 m/s<sup>2</sup> (e.g., Dry asphalt road [45]), and the emergency braking deceleration is 10 m/s<sup>2</sup> [32], [46]. The vehicle length is 4.3 m. In Group1, Group2, and Group3, new vehicles are generated and enter the lane at the rate of 1 vehicle/second in the first 360 s, 480 s, and 720 s, respectively with the initial velocity of 30 m/s (108 km/h), 20 m/s (72 km/h), and 10 m/s (36 km/h), respectively. Then, each vehicle updates the speed every 10 ms, and the speed of all vehicles follows the uniform distribution for the mean speed. The traffic will last for 720 s, 800 s, and 1500 s in Group1, Group2, and Group3, respectively. The positions of vehicles are recorded at the sample step of 1 ms. Fig. 6 shows changing vehicles density with time in the shaded segment of Fig. 5. It can be seen that the vehicle density is stable within the time interval [200, 400] s for Group1, [260, 520] s for Group2, and [540, 800] s for Group3, respectively. At the same time, we calculate the average vehicle density when the traffic is stable as shown in Table II. It is not difficult to see that the higher the average vehicle speed, the lower the vehicle density. Otherwise, the smaller the average vehicle speed, the greater the vehicle density.

### C. The speed-density relationship

Greenshields model [41] built the linear relationship between the vehicle speed and density under uninterrupted flow conditions. The vehicle speed and vehicle density generated by SUMO are as shown in Table II. We assume that the vehicle density is independent of the vehicle speed [33], [34]. Then, we do linear regression (Goodness of Fit  $R^2 = 0.9774$ ) with the data points and the Greenshields model to get the formula below.

$$V = -102.89\beta + 38.177 \quad (9)$$

where  $\beta$  is the density,  $V$  is the speed.

### D. Comparison between mobility and stationary scenes simulations

Take the mobility traffic in Group1 as the example, we feed the sumo record in the shaded segment of Fig. 5 at the interval [200, 400] s into the NS2 and set every vehicle as the

TABLE II: The vehicle speed and vehicle density calculated in SUMO

	Mean speed (m/s)	Maximum speed (m/s)	Minimum speed (m/s)	Average density calculated (vehicles/meter)
Group1	30	33	27	0.09
Group2	20	22	18	0.16
Group3	10	11	9	0.28

broadcast node running the periodic message broadcast and reception obeying IEEE 802.11p and compute the PRPs and PRRs. At the same time, we generate the stationary scenario, i.e., vehicles are placed according to HPP with the density of 0.09 vehicles/meter at a road with a length of 10000 m in NS2. Fig. 7 shows the PRP and PRR comparisons between the mobility and stationary scenarios simulations. We find that the PRPs and PRRs in the stationary scenario simulation are almost the same as the mobility scenario simulation. In this way, next, we adopt a stationary scene simulation, which is equivalent to a mobility scene simulation of same density.

### E. Comparison between different PHY layer strategies

NS2 has implemented the capture effect, which could be turned on or off with a boolean parameter. At the same time, we implement SIC in the PHY module of NS2. Herein, we assume that SIC is perfectly implemented without considering hardware implementation details. Then, we compare PRPs and PRRs between different PHY layer strategies while the conventional CSMA as MAC layer as shown in Fig. 8. The density is 0.1 vehicles/meter, the beacon rate is 10 Hz. The results show that the system with SIC or capture enabled outperform those without an advanced PHY layer mechanism, especially when the receiving distance is less than 70 m. At a farther distance, their results are almost the same. Compare with the original PHY layer strategy, the capture increases the reception rates at ranges close to the sender. The same comparisons between the original PHY layer strategy and capture enabled have been witnessed in Fig. 10 of [35]. The PHY layer strategy enabled SIC behaves similarly to capture

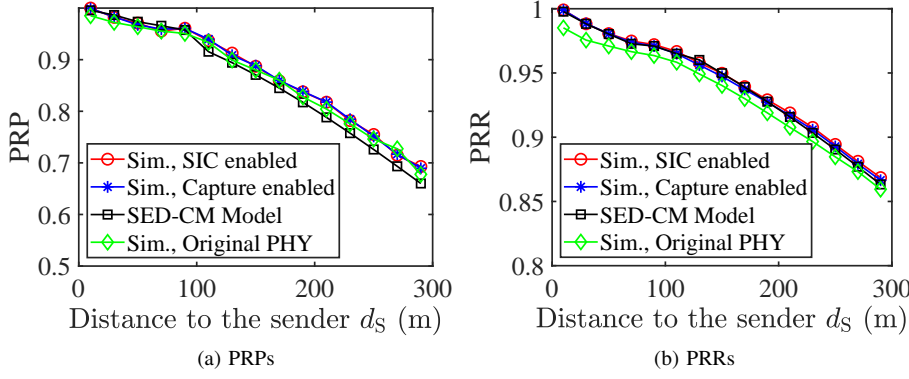


Fig. 8: PRPs and PRRs comparisons between different PHY layer strategies as well obtained from NS2 simulation as the model

enabled since the conventional CSMA could not effectively exploit the SIC capability [30]. Moreover, we compare the PRPs and PRRs between the proposed SED-CM model and the simulations with different PHY layer strategies as shown in Fig. 8. The analytical results present consistency with the results of the capture or SIC enabled simulations. In this way, the model could be applied to the systems supporting SIC or capture effect when conventional CSMA as MAC layer.

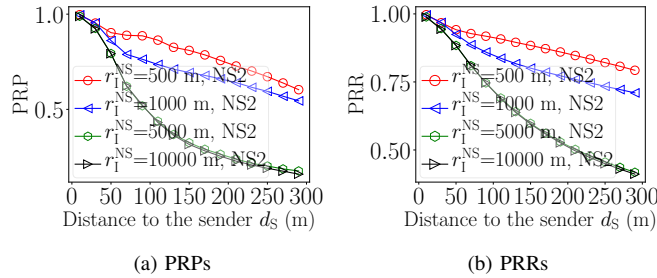


Fig. 10: PRPs and PRRs comparisons between NS2 simulations with different interference ranges

#### IV. MAXIMUM INTERFERENCE RANGE SETTING

In NS2, we could control the minimum interference power by the parameter  $PowerMonitorThresh_{-}$ , which is denoted by  $I_{th}$ . Similar to Eq. (8), the interference range  $r_1^{NS}$  in NS2 can be calculated according to the path loss law, as follows.

$$r_1^{NS} = d_0 \sqrt[4]{P_t G_t G_r \eta / I_{th}}. \quad (10)$$

At the same time, we modify NS2 source code to record interference nodes of packets arriving at a receiver, -1 if there is no interference. In this way, the interference distance  $d_I$  could be calculated by the coordinates of the receiver and the interferer. We can further obtain the distribution of the interference distance. Specifically, we run 38 groups of simulation experiments corresponding to 38 densities ranging from 0.01 vehicles/meter to 0.77 vehicles/meter with an interval of 0.02. In these simulation experiments, the simulation scenario is set as a circular lane with a 10000 m perimeter. The nodes are placed on the lane obeying HPP distribution with the given density. The packet generation rate is 10 Hz, the data rate

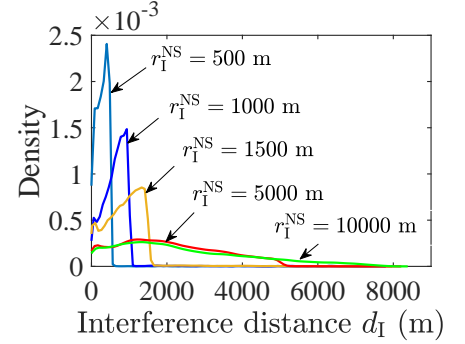


Fig. 9: Interference distance distribution

is 24 Mbps, the noise power is -99 dBm, and the sensing range is 500 m. Each group of the experiment includes five simulations with different interference ranges  $r_1^{NS}$ , 500 m, 1000 m, 1500 m, 5000 m, and 10000 m, respectively. Then we write Python programs to count the interference distance  $d_I$ , PRP, and PRR according to the trace file and node position file. Moreover, kernel density estimation (KDE) is used to estimate interference distance distribution based on the simulation data.

Fig. 9 compares the distribution of the interference distance between different interference ranges at the density of 0.1 vehicles/meter. Other densities are similar. It could be seen from a curve that most interference distances are smaller than or equal to the interference range calculated by (10). Comparing the different curves, it is obvious that the distribution of the interference distance changes significantly with the interference range when the interference range is less than 5000 m. However, after 5000 m, there is very little discrepancy between the two curves representing the distribution of the interference distance for the interference range of 5000 m and 10000 m. Moreover, Fig. 10 presents the PRPs and PRRs with different interference ranges. We find that the results for the interference range of 10000 m and 5000 m are almost completely consistent. PRPs and PRRs no longer decrease as the interference range increases after 5000 m. The occurrence of this phenomenon is connected to two aspects. On the one hand, as shown in Fig. 9, most of the interference fall in the range [0, 5000] m in the case of interference range of 10000 m. On the other hand, the interference power is too small for nodes that are too far away, which has almost no effect on the SINR. Without loss of generality, we adopt  $I_{max}$  to denote such interference range after which the distribution of interference distance changes slightly, such as 5000 m as shown in Fig. 9. Thus, the potential maximum interference range  $r_1$  should be the minimum between  $r_1^{NS}$  and  $I_{max}$ , which is expressed as shown in (5).

#### V. RELIABILITY EVALUATION

The assumption of the SINR related interference range corresponds to where the interference will deterministically make the SINR less than the threshold and thus the reception fails,

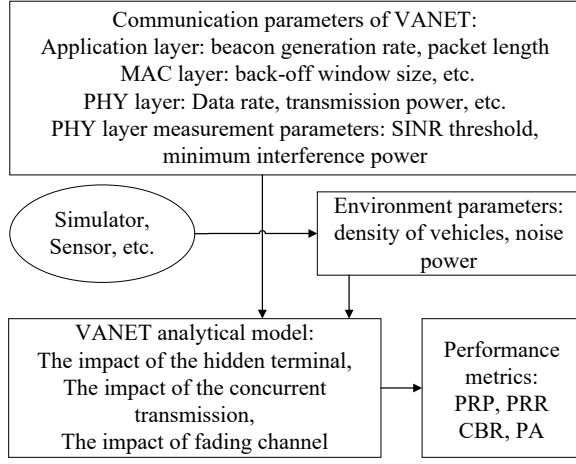


Fig. 11: The overall framework of the SED-CM model for 802.11p VANET reliability evaluation

which facilitates efficient and effective analysis of QoS metrics by considering the size of the interference range and the transmission probability of the node in steady-state. On the top of the SINR related effective interference range, the proposed SED-CM model introduces the maximum interference range as the upper limit of the SINR related interference range. In this way, the analysis of the interference is more precise since the effect of the minimum interference power that determines the maximum interference range is taken into account. The section starts with the overall framework. Then, we give a series of mathematical derivations for the evaluation of PRP, PRR, CBR and PA.

### A. Overall framework

The overall framework of the SED-CM model is shown in Fig. 11. Two types of parameters are fed to the analytical model. One is the communication parameters used in Application, MAC, and PHY layers. Herein, the SINR threshold and minimum interference power are treated as PHY layer parameters, which need to be measured in the actual device. The other is the environment parameters including the vehicle density and noise power. The density of vehicles represents the traffic condition, which can be evaluated by a simulator, sensor, etc.. Based on these parameters, the model separately evaluates the effects of hidden terminals, concurrent transmission, and fading. PRP, PRR, CBR and PA are further derived. In the model, we adopt the semi-Markov process (SMP) model [9] to calculate the steady-state probability  $\pi_{XMT}$  that the node is in the transmitting state, the hidden terminal transmission probability  $p_t$  during the vulnerable period [9] of the tagged vehicle, and the probability  $\pi_0$  that a neighbor starts to transmit a packet at the beginning of the same time slot with the tagged vehicle.

### B. PRP evaluation

PRP [10] is defined as the probability that a node at a distance of  $d_S$  successfully receives a packet from a transmitter, which is evaluated as the probability that the conditional SINR

measured at the receiver is higher than the given threshold and the receiving power is greater than the receiving power threshold. The probability analysis is done based on the assumption that the hidden terminals, concurrent transmissions, and fading are independent of each other [14]. In this way, we could approximate PRP by analyzing the effect of hidden terminals, concurrent transmissions, and fading, respectively.

1) *PRP considering the hidden terminal*: The SINR is simplified to a SIR in the presence of interference. The two shaded segments (The same side with "r" and without "r" counts as one) in both sides of Fig. 2 present the hidden terminal areas, which are beyond the sensing range of the tagged transmitter. Two cases are used to analyze the impact of hidden terminals on PRP. The first case is that the transmission of only one hidden terminal could make SIR less than the threshold. In this case, the farthest distance between the receiver and the interferer is  $r_I^{\text{Eff}-1}$ , not more than  $r_I$ . We count the sizes of such hidden terminal areas (corresponding to the length of the shaded area with "r"), including the left and right sides, as follows.

$$\begin{aligned} L_{ht}^1 &= \max(\min(r_I^{\text{Eff}-1}, r_I) - r_E + d_S, 0) \\ L_{ht}^2 &= \max(\min(r_I^{\text{Eff}-1}, r_I) - r_E - d_S, 0) \end{aligned} \quad (11)$$

Then, we evaluate PRP in this case by calculating the probability that no transmission causes SIR to be less than the given threshold.

$$\text{PRP}_{ht}^{E1} = 1 - \Pr(\text{SIR} < \theta | d_S) = \exp(-\beta p_t (L_{ht}^1 + L_{ht}^2)). \quad (12)$$

The second possible case is that the transmissions of two nodes (one within the left hidden terminal area and another within the right hidden terminal area) cause the SIR to be less than the given threshold. Thus, the probability that the SIR is greater than the given threshold is equal to the probability that no such two nodes are transmitting at the same time. In this case, the farthest distance between the receiver and the interferer is  $r_I^{\text{Eff}-2}$ , greater than  $r_I^{\text{Eff}-1}$ , and less than  $r_I$ . The sizes  $L_{ht}^{21}$  and  $L_{ht}^{22}$  of such hidden terminal areas (corresponding to the length of the shaded area without "r") on the right and left are calculated by (13) and (14), respectively.

$$L_{ht}^{21} = \max(\min(r_I^{\text{Eff}-2}, r_I) - \max(r_I^{\text{Eff}-1}, r_E - d_S), 0) \quad (13)$$

$$L_{ht}^{22} = \max(\min(r_I^{\text{Eff}-2}, r_I) - \max(r_I^{\text{Eff}-1}, r_E + d_S), 0) \quad (14)$$

Then, we obtain the expression of PRP in the case as follows.

$$\begin{aligned} \text{PRP}_{ht}^{E2} &= 1 - \Pr(\text{SIR} < \theta | d_S) \\ &= 1 - (1 - \exp(-\beta p_t L_{ht}^{21}))(1 - \exp(-\beta p_t L_{ht}^{22})) \end{aligned} \quad (15)$$

2) *PRP considering the concurrent transmission*: Concurrent transmission area refers to the segment in the range of  $(-r_E, r_E)$  centered at the transmitter. Similar to the analysis of the hidden terminals, we evaluate PRP considering the concurrent transmission in two cases. The first case is that the transmission of a node in the concurrent transmission area makes the reception fail, that is, the farthest distance between the receiver and the interferer is  $r_I^{\text{Eff}-1}$ , no more than  $r_I$ .

Then, we have the size of such concurrent transmission area, including the right and left sides as follows.

$$\begin{aligned} L_{cc}^1 &= \min(\min(r_I^{\text{Eff}-1}, r_I), r_E - d_S) \\ L_{cc}^2 &= \min(\min(r_I^{\text{Eff}-1}, r_I), r_E + d_S) \end{aligned} \quad (16)$$

Then, we evaluate PRP in this case.

$$\text{PRP}_{cc}^{\text{E1}} = 1 - \Pr(\text{SIR} < \theta | d_S) = \exp(-\pi_0 \beta (L_{cc}^1 + L_{cc}^2)) \quad (17)$$

The second case is that the transmission of two nodes on the left and right side respectively in the concurrent transmission area makes the reception fail, that is, the farthest distance between the receiver and the interferer is  $r_I^{\text{Eff}-2}$ , greater than  $r_I^{\text{Eff}-1}$ , and less than  $r_I$ . In this case, the sizes  $L_{cc}^{21}$  and  $L_{cc}^{22}$  of such concurrent transmission areas on the right and left are as follows, respectively.

$$L_{cc}^{21} = \max(\min(\min(r_I^{\text{Eff}-2}, r_I), r_E - d_S) - r_I^{\text{Eff}-1}, 0) \quad (18)$$

$$L_{cc}^{22} = \max(\min(\min(r_I^{\text{Eff}-2}, r_I), r_E + d_S) - r_I^{\text{Eff}-1}, 0) \quad (19)$$

Then, we calculate PRP in this case.

$$\begin{aligned} \text{PRP}_{cc}^{\text{E2}} &= 1 - \Pr(\text{SIR} < \theta | d_S) \\ &= 1 - (1 - \exp(-\pi_0 \beta L_{cc}^{21}))(1 - \exp(-\pi_0 \beta L_{cc}^{22})) \end{aligned} \quad (20)$$

3) *PRP considering the imperfect channel with fading and noise*: Considering Nakagami fading model [39], [40], the PDF of the receiving power  $P_r$  at a receiver with  $d$  away from the transmitter [14] is

$$f_{P_r|d}(x) = \frac{1}{\Gamma(m)} \left( \frac{m}{\omega(d)} \right)^m x^{m-1} \exp\left(-\frac{mx}{\omega(d)}\right) \quad (21)$$

In the absence of interference, SINR is simplified to signal-to-noise ratio (SNR). We have  $\text{SNR} = P_r/N_0$ , where  $N_0$  denotes the noise power. According to (21), we obtain the PDF of SNR as follows.

$$f_{\text{SNR}|d}(y) = \frac{(N_0 m)^m}{\Gamma(m) \omega^m} (N_0 y)^{(m-1)} \exp\left(-\frac{m N_0 y}{\omega}\right) \quad (22)$$

Then, known  $P_{th}$  is receiving power threshold,  $\theta$  is the SNR threshold. Without loss of generality, we could rewrite the two reception conditions into one based on the SNR, i.e.,  $\text{SNR} \geq \max(\theta, P_{th}/N_0)$ . In this way, we calculate PRP in the case of no interference as follows.

$$\begin{aligned} \text{PRP}_F &= \Pr(\text{SNR} \geq \max(\theta, \frac{P_{th}}{N_0}) | d_S) \\ &= 1 - \Pr(\text{SNR} < \max(\theta, \frac{P_{th}}{N_0}) | d_S) \\ &= \begin{cases} 1 - \frac{(N_0 m)^m}{\Gamma(m) \omega^m} \int_0^\theta z^{m-1} \exp(-N_0 (\frac{m}{\omega}) z) dz, & \theta \geq \frac{P_{th}}{N_0} \\ 1 - \frac{(N_0 m)^m}{\Gamma(m) \omega^m} \int_0^{\frac{P_{th}}{N_0}} z^{m-1} \exp(-N_0 (\frac{m}{\omega}) z) dz, & \theta < \frac{P_{th}}{N_0} \end{cases} \\ &= \begin{cases} 1 - \frac{(N_0 m)^m}{\Gamma(m)} \int_0^{\frac{\theta}{\omega}} z^{m-1} \exp(-N_0 m z) dz, & \theta \geq \frac{P_{th}}{N_0} \\ 1 - \frac{(N_0 m)^m}{\Gamma(m)} \int_0^{\frac{P_{th}}{N_0 \omega}} z^{m-1} \exp(-N_0 m z) dz, & \theta < \frac{P_{th}}{N_0} \end{cases} \end{aligned} \quad (23)$$

$P_{th}$  is the average receiving power at the distance  $r_E$  away from the transmitter.  $\theta N_0$  is the average receiving power at the communication distance  $R_c$ . According to the path loss, we have:

$$\frac{\theta N_0}{P_{th}} = \left(\frac{r_E}{R_c}\right)^\alpha, \quad \frac{\theta N_0}{\omega(d_S)} = \left(\frac{d_S}{R_c}\right)^\alpha \quad (24)$$

Then,

$$\frac{\theta}{\omega(d_S)} = \frac{\theta}{P_{th}} \left(\frac{d_S}{r_E}\right)^\alpha \quad (25)$$

and

$$\frac{P_{th}}{N_0 \omega(d_S)} = \frac{1}{N_0} \left(\frac{d_S}{r_E}\right)^\alpha \quad (26)$$

By applying (25) and (26) in (23), we have

$$\begin{aligned} \text{PRP}_F &= \begin{cases} 1 - \frac{(N_0 m)^m}{\Gamma(m)} \int_0^{\frac{\theta}{P_{th}} \left(\frac{d_S}{r_E}\right)^\alpha} z^{m-1} e^{-N_0 m z} dz, & \theta \geq \frac{P_{th}}{N_0} \\ 1 - \frac{(N_0 m)^m}{\Gamma(m)} \int_0^{\frac{1}{N_0} \left(\frac{d_S}{r_E}\right)^\alpha} z^{m-1} e^{-N_0 m z} dz, & \theta < \frac{P_{th}}{N_0} \end{cases} \\ &= \begin{cases} 1 - \frac{1}{\Gamma(m)} \gamma\left(m, \frac{N_0 m \theta}{P_{th}} \left(\frac{d_S}{r_E}\right)^\alpha\right), & \theta \geq \frac{P_{th}}{N_0} \\ 1 - \frac{1}{\Gamma(m)} \gamma\left(m, m \left(\frac{d_S}{r_E}\right)^\alpha\right), & \theta < \frac{P_{th}}{N_0} \end{cases} \end{aligned} \quad (27)$$

where  $\gamma(s, x) = \int_0^x t^{s-1} e^{-t} dt$  is the lower incomplete gamma function.

The evaluation of PRP can be combined as follows.

$$\text{PRP}(d_S) = \text{PRP}_{ht}^{\text{E1}} \times \text{PRP}_{ht}^{\text{E2}} \times \text{PRP}_{cc}^{\text{E1}} \times \text{PRP}_{cc}^{\text{E2}} \times \text{PRP}_F \quad (28)$$

### C. PRR evaluation

PRR [10] is also the function of the receiving distance and is defined as the percentage of nodes that successfully receive a packet from the tagged transmitter among the receivers. Therefore, PRR can be written as a function of PRP, as follows:

$$\text{PRR}(d_S) = \frac{\int_0^{d_S} \beta \text{PRP}(x) dx}{\beta d_S} = \frac{1}{d_S} \int_0^{d_S} \text{PRP}(x) dx \quad (29)$$

### D. Channel busy ratio

Channel busy ratio (CBR) is defined as the percentage of busy time duration within certain observation period [2], which has been given by [2]

$$\text{CBR} = 2r_E \beta \frac{T}{T_c} \left(1 - \frac{p_{dc}}{2} - \frac{p_{dh}}{4}\right) \quad (30)$$

where  $T$  is a packet transmission time, which is made up of the packet header transmission time  $T_H$ , the packet body transmission time  $E[\text{PL}]/R_d$  and the propagation delay  $\delta$ . We have  $T = T_H + E[\text{PL}]/R_d + \delta$ .  $T_c$  is the packet generation interval.  $p_{dc}$  is the probability that at least one more transmission occurs in the carrier sensing range of an observer in the channel. We have  $p_{dc} = 1 - (1 - \pi_0)^{2\beta r_E}$  [2].  $p_{dh}$  is the probability that at least two hidden terminal transmissions are overlapped from the perspective of an observer in the channel. We have  $p_{dh} = (1 - (1 - p_t)^{\beta r_E/2})^2$  [2].

### E. The awareness probability

The awareness probability (PA) [2] is the reliability metric in the application level, which could be used to estimate whether the current channel can meet the reliability requirements of safety applications or not. It refers to the probability of successfully receiving at least  $n$  packets in the tolerance time window  $T_a$ .

$$P_A(x, n, T_a) = \sum_{k=n}^{\lfloor \frac{T_a}{T_c} \rfloor} \binom{\lfloor \frac{T_a}{T_c} \rfloor}{k} \text{PRP}(x)^k (1 - \text{PRP}(x))^{\lfloor \frac{T_a}{T_c} \rfloor - k} \quad (31)$$

where  $T_a$  changes with the speed of the vehicle and the specific application.

TABLE III: The QoS requirements of typical safety applications

Application	$T_a$	Distance	$n$	The requirement of PA
CCW	-	400 m	1	99.0%
SVI	-	100 m	3	99.9%
RCW	-	50 m	5	99.9%

Table III gives the stringent QoS requirements of three BSM based safety applications, cooperative collision warning (CCW), slow vehicle indication (SVI), and rear-end chain collision warning (RCW), respectively. Inspired by [32], we calculate the  $T_a$  in the emergency state as the value of  $T_a$ . Considering the vehicle in front stops, the time for notifying the following car to not collide is  $T_a$ , as follows.

$$T_a = \frac{vT_{hw} - d_{br}}{v} = T_{hw} - \frac{v}{2a} \quad (32)$$

where  $T_{hw}$  is the time headway. A time headway of 1.5-2 s has been found to provide sufficient safety margin to avoid collisions with the lead vehicle in an emergency condition [47]–[49].  $d_{br}$  is the braking distance and  $d_{br} = \frac{v^2}{2a}$ ,  $a$  is the emergency braking deceleration in  $\text{m/s}^2$ . The equation shows that the more the speed, the less the tolerable time window.

## VI. EXTEND TO THE INTERSECTION SCENARIO

In the section, we extend the SED-CM model to evaluate the reliability at an intersection. The intersection scenario analysis is more complex than 1D since more interference areas need to be considered. Two cases accounting for locations geometry between the tagged transmitter and receiver at the intersection scenario could be analyzed [12]. The sender and receiver are on the same road, and the sender and receiver are on different roads. Herein, we present the derivation process when the sender and the receiver are on different roads. The derivation process in another case could be similarly given.

The interference scenario under consideration is shown in Fig. 12. The origin is set at the road intersection. The tagged sender  $S_1$  is located at coordinate  $(x_s, 0)$ . One of the receivers  $R_{S_1}$  is at coordinate  $(0, y_r)$ , and the distance between  $R_{S_1}$  and  $S_1$  is  $d_S$ .  $S_2$ ,  $S_3$ ,  $S_4$ , and  $S_5$  present the interferers at the left, up, right, and down sides, respectively. (27) for PRP considering the impact of fading channel, (28) for PRP computation, (29) for PRR computation, (30) for

CBR derivation, and (31) for PA derivation are the same in the intersection scenario as the 1D Highway scenario. We need to derive PRP considering the hidden terminal and PRP considering the concurrent transmissions in the intersection scenario.

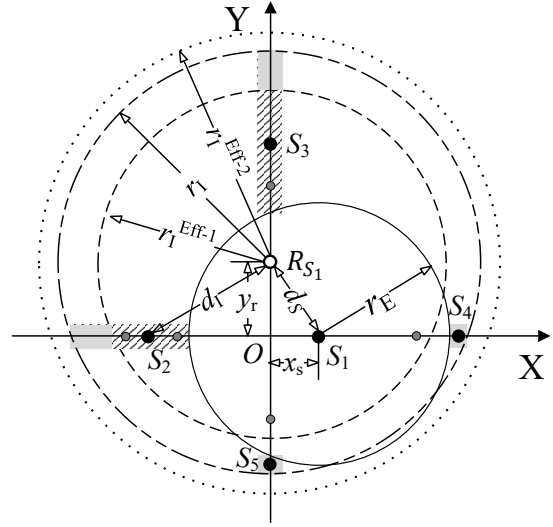


Fig. 12: Interference scenario at an intersection, the sender is at X-axis, and the receiver is at Y-axis

1) *PRP considering the hidden terminal*: The SINR is simplified to SIR in the presence of interference. The four shaded segments in Fig. 12 present the hidden terminal areas in the four directions. The first case is that the transmission of only one hidden terminal could make SIR less than the threshold. We count the sizes of such hidden terminal areas (corresponding to the length of the shaded area with "r"), the left, right, up, and down sides, respectively, as follows.

$$\begin{aligned} L_{ht}^1 &= \max(\sqrt{(\min(r_I^{\text{Eff}-1}, r_I))^2 - y_r^2} - r_E + x_s, 0) \\ L_{ht}^2 &= \max(\sqrt{(\min(r_I^{\text{Eff}-1}, r_I))^2 - y_r^2} - r_E - x_s, 0) \\ L_{ht}^3 &= \max(\min(r_I^{\text{Eff}-1}, r_I) - \sqrt{r_E^2 - x_s^2 - y_r}, 0) \\ L_{ht}^4 &= \max(\min(r_I^{\text{Eff}-1}, r_I) - \sqrt{r_E^2 - x_s^2 + y_r}, 0) \end{aligned} \quad (33)$$

Then, we evaluate PRP in this case.

$$\text{PRP}_{ht}^{\text{E1}} = 1 - \Pr(\text{SIR} < \theta | d_S) = \exp(-\beta p_t (L_{ht}^1 + L_{ht}^2 + L_{ht}^3 + L_{ht}^4)). \quad (34)$$

The second possible case is that the transmissions of at least two nodes in two sides cause the SIR to be less than the given threshold. The sizes of such hidden terminal areas (corresponding to the length of the shaded area without "r") on the left, right, up, and down sides are  $L_{ht}^{21}$ ,  $L_{ht}^{22}$ ,  $L_{ht}^{23}$ , and  $L_{ht}^{24}$ , respectively, as follows.

$$L_{ht}^{21} = \max(\sqrt{(\min(r_I^{\text{Eff}-2}, r_I))^2 - y_r^2} - \max(\sqrt{(r_I^{\text{Eff}-1})^2 - y_r^2}, r_E + x_s), 0) \quad (35)$$

$$L_{ht}^{22} = \max(\sqrt{(\min(r_I^{\text{Eff}-2}, r_I))^2 - y_r^2} - \max(\sqrt{(r_I^{\text{Eff}-1})^2 - y_r^2}, r_E - x_s), 0) \quad (36)$$

$$L_{ht}^{23} = \max(\min(r_I^{\text{Eff}-2}, r_I) - \max(r_I^{\text{Eff}-1}, \sqrt{r_E^2 - x_s^2 - y_r}), 0) \quad (37)$$

$$L_{ht}^{24} = \max(\min(r_I^{\text{Eff}-2}, r_I) - \max(r_I^{\text{Eff}-1}, \sqrt{r_E^2 - x_s^2 + y_r}), 0) \quad (38)$$

Then, we obtain the expression of PRP in the case as follows.

$$\begin{aligned} \text{PRP}_{ht}^{\text{E2}} &= 1 - \Pr(\text{SIR} < \theta | d_S) = 1 - \prod_{i=1}^4 (1 - \exp(-\beta p_t L_{ht}^{2i})) \\ &- \sum_{i=1}^4 \left[ \exp(-\beta p_t L_{ht}^{2i}) \prod_{j=1, j \neq i}^4 (1 - \exp(-\beta p_t L_{ht}^{2j})) \right] \\ &- \sum_{i=1}^3 \left[ \sum_{j=i+1}^4 \exp(-\beta p_t L_{ht}^{2i}) \exp(-\beta p_t L_{ht}^{2j}) \right. \\ &\quad \left. \prod_{k=1, k \neq i, j}^4 (1 - \exp(-\beta p_t L_{ht}^{2k})) \right] \end{aligned} \quad (39)$$

2) *PRP considering the concurrent transmission:* Similar to analysis for the 1D, we evaluate PRP considering the concurrent transmission in two cases. The first case is that a node's transmission in the concurrent transmission area makes the reception fail. We have the sizes of such concurrent transmission areas, including the left, right, up, and down sides as follows.

$$\begin{aligned} L_{cc}^1 &= \min(\sqrt{\min(r_I^{\text{Eff}-1}, r_I)^2 - y_r^2}, r_E + x_s) \\ L_{cc}^2 &= \min(\sqrt{\min(r_I^{\text{Eff}-1}, r_I)^2 - y_r^2}, r_E - x_s) \\ L_{cc}^3 &= \min(\min(r_I^{\text{Eff}-1}, r_I), \sqrt{r_E^2 - x_s^2 - y_r}) \\ L_{cc}^4 &= \min(\min(r_I^{\text{Eff}-1}, r_I), \sqrt{r_E^2 - x_s^2 + y_r}) \end{aligned} \quad (40)$$

Then, we evaluate PRP in this case.

$$\text{PRP}_{cc}^{\text{E1}} = 1 - \Pr(\text{SIR} < \theta | d_S) = \exp(-\pi_0 \beta (L_{cc}^1 + L_{cc}^2 + L_{cc}^3 + L_{cc}^4)) \quad (41)$$

The second case is that the transmission of at least two nodes on two sides in the concurrent transmission area makes the reception fail. In this case, the sizes of such concurrent transmission areas on the left, right, up, and down sides are  $L_{cc}^{21}, L_{cc}^{22}, L_{ht}^{23}, L_{ht}^{24}$ , respectively, as follows.

$$\begin{aligned} L_{cc}^{21} &= \max(\min(\sqrt{(\min(r_I^{\text{Eff}-2}, r_I))^2 - y_r^2}, r_E + x_s) \\ &- \sqrt{(r_I^{\text{Eff}-1})^2 - y_r^2}, 0) \end{aligned} \quad (42)$$

$$\begin{aligned} L_{cc}^{22} &= \max(\min(\sqrt{(\min(r_I^{\text{Eff}-2}, r_I))^2 - y_r^2}, r_E - x_s) \\ &- \sqrt{(r_I^{\text{Eff}-1})^2 - y_r^2}, 0) \end{aligned} \quad (43)$$

$$L_{cc}^{23} = \max(\min(\min(r_I^{\text{Eff}-2}, r_I), \sqrt{r_E^2 - x_s^2 - y_r}) - r_I^{\text{Eff}-1}, 0) \quad (44)$$

$$L_{cc}^{24} = \max(\min(\min(r_I^{\text{Eff}-2}, r_I), \sqrt{r_E^2 - x_s^2 + y_r}) - r_I^{\text{Eff}-1}, 0) \quad (45)$$

Then, we have  $\text{PRP}_{cc}^{\text{E2}}$  in the intersection scenario.

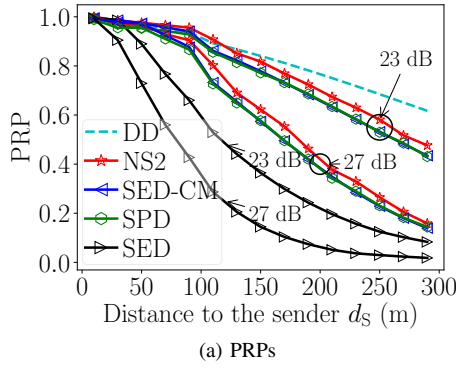
$$\begin{aligned} \text{PRP}_{cc}^{\text{E2}} &= 1 - \Pr(\text{SIR} < \theta | d_S) = 1 - \prod_{i=1}^4 (1 - \exp(-\beta p_t L_{cc}^{2i})) \\ &- \sum_{i=1}^4 \left[ \exp(-\beta p_t L_{cc}^{2i}) \prod_{j=1, j \neq i}^4 (1 - \exp(-\beta p_t L_{cc}^{2j})) \right] \\ &- \sum_{i=1}^3 \left[ \sum_{j=i+1}^4 \exp(-\beta p_t L_{cc}^{2i}) \exp(-\beta p_t L_{cc}^{2j}) \right. \\ &\quad \left. \prod_{k=1, k \neq i, j}^4 (1 - \exp(-\beta p_t L_{cc}^{2k})) \right] \end{aligned} \quad (46)$$

## VII. EXPERIMENTS

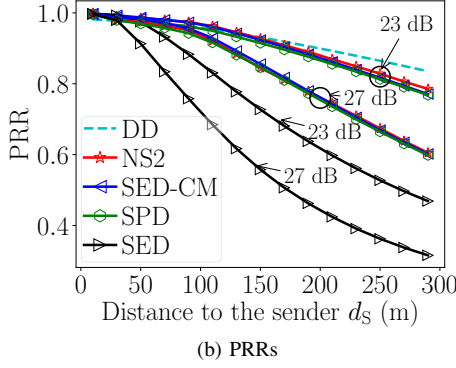
In the section, we present the experiment results from the theoretical models and NS2 simulation and make a considerable analysis. We first compare the proposed SINR related Effective Distance Constrained by the Maximum interference range-based (SED-CM) model and the Deterministic Distance-based (DD) model, the SINR Probability Derivation-based (SPD) model, and the SINR related Effective Distance-based (SED) model in the 1D scenario. The comparison results show that the SED-CM model has the best evaluation capacity while changing the maximum interference range. The cross-validation experiments between the SED-CM model and NS2 simulation in the 1D scenario are also be conducted. The cross-validation results show that the error is small in the case of the interference range being small or the interference range being large. However, the error is larger in the medium level interference range. Second, we present the cross-validation results at the intersection scenario. The results are similar to the 1D scenario. The conclusion in the 1D scenario is adopted to explain the intersection scenario. Third, we analyze the impact of the hidden terminal, which can be reduced by decreasing the beacon rate or increasing the sensing range individually or in combination. Finally, we analyze the impact of speed on the performance of VANET by comprehensively considering the channel busy rate and the awareness probability of safety applications.

### A. PRPs and PRRs in the 1D scenario

1) *Compare with the previous models:* We set the 1D scene as a circle with a perimeter of 10000 m. The density is 0.1 vehicles/meter. The other parameter settings are shown in Table I. The PRPs and PRRs at 15 receiving distances from 10 m to 290 m at an interval of 20 m are computed. Fig. 13 and Fig. 14 present PRPs and PRRs comparisons between the NS2 simulations, SED-CM, DD, SPD, and SED models. Fig. 13 is plotted according to the data when  $r_I$  equals 500 m and SINR threshold  $\theta$  equals 23 dB and 27 dB. Fig. 14 is plotted for  $r_I$  of 5000 m and the same SINR thresholds as Fig. 13. We can find that PRPs and PRRs present decreasing trends with the increase in the receiving distance  $d_S$ , corresponding to the reason behind the larger the receiving distance, the smaller

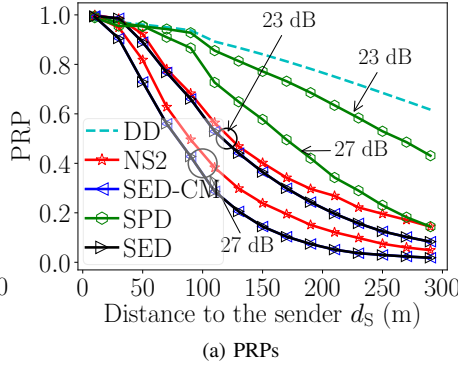


(a) PRPs

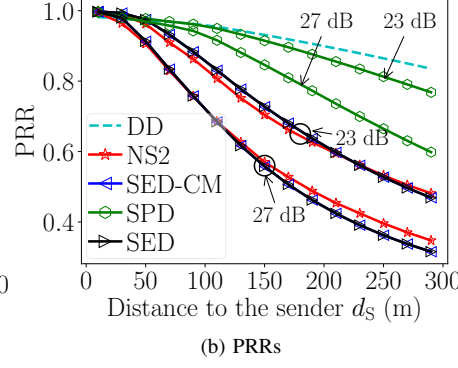


(b) PRRs

Fig. 13: Comparisons between four models and NS2, 1D scenario,  $r_I = 500$  m

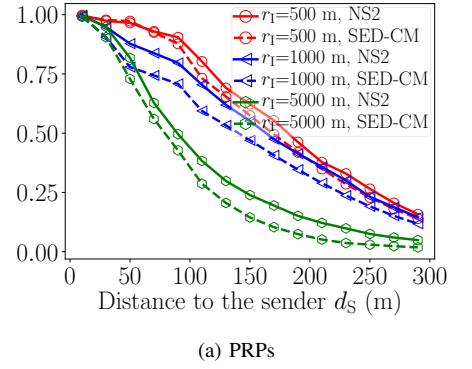


(a) PRPs

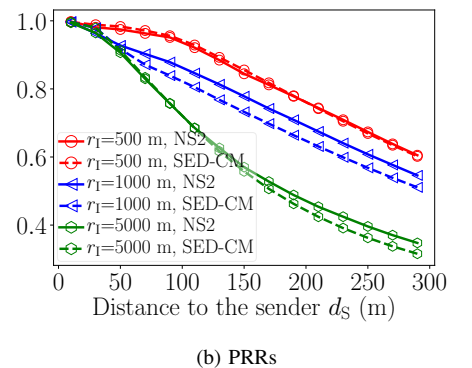


(b) PRRs

Fig. 14: Comparisons between four models and NS2, 1D scenario,  $r_I = 5000$  m



(a) PRPs



(b) PRRs

Fig. 15: Comparisons between the SED-CM model and NS2, 1D scenario, changing  $r_I$

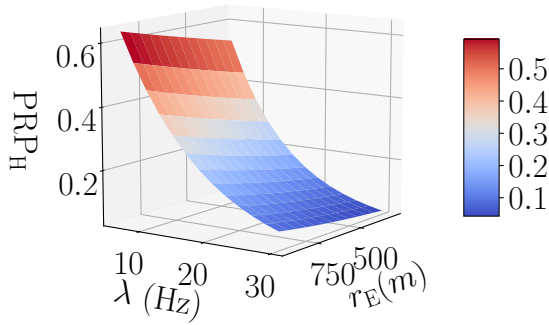


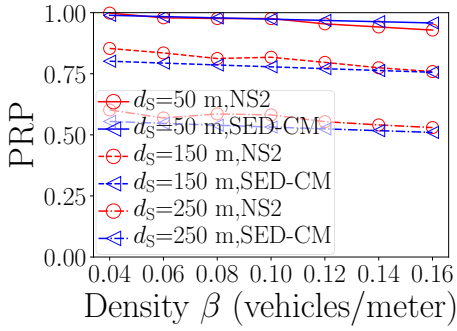
Fig. 16: The impact of the hidden terminal v.s. beacon rate and sensing range, 1D scenario

the receiving power, and the smaller the SINR. More packets will be discarded. It can be seen that the greater the SINR threshold, the smaller the PRPs and PRRs as shown in Fig. 13 and Fig. 14. Because increasing the SINR threshold makes the reception condition more stringent.

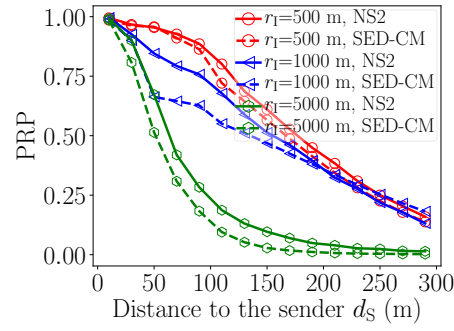
As mentioned in Section I-B, interference range equals sensing range of 500 m in the DD model. Results of the DD model are not related to the SINR threshold. In this way, the theoretical results of the DD model show the significant errors with those of NS2 simulation, as shown in Fig. 13 and Fig. 14. Fig. 13 shows that the PRPs and PRRs of the SPD and the proposed SED-CM models can fit well with those of NS2 simulation when  $r_I$  equals 500 m. However,

the results of the SED model [2] are much worse than those of NS2 simulation because of the larger interference range used. Fig. 14 shows that the PRPs and PRRs of the SPD model are much better than the NS2 simulation results when  $r_I$  equals 5000 m. Because the interference range considered by the SPD model is much less than 5000 m, the impact of interference is underestimated. At the same time, the SED and the proposed SED-CM models perform in agreement with the NS2 simulation. In summary, the SPD model could provide accuracy estimation in the case of the interference range is approximate  $r_E$  (i.e., 500 m), but it is not suitable for a larger interference range. At the same time, the computational complexity of the SPD model is too high to be extended to the scenario with a larger interference range. The SED model could provide accuracy estimation in the case of the interference range is greater (such as 5000 m), but it did not fit for the case with the less interference range. The proposed SED-CM model could cover both cases mentioned above.

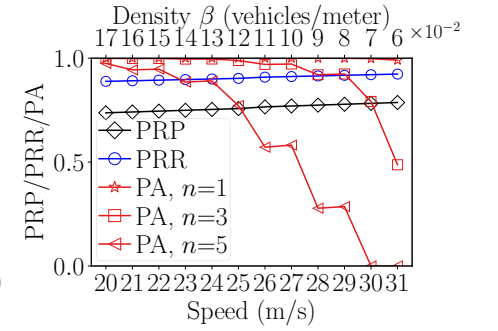
2) *The cross-validation with NS2:* Fig. 15 shows the PRPs and PRRs comparison between the SED-CM model and NS2 simulation with different maximum interference ranges. The larger the maximum interference range, the more interference, thus, PRPs and PRRs present decreasing trend with the increasing interference range. Because more interference reduces the value of SINR. At the same time, We could witness that the discrepancy between the model and the simulation are larger when the interference range equals 1000 m than the interference range of 500 m and 5000 m. The interference



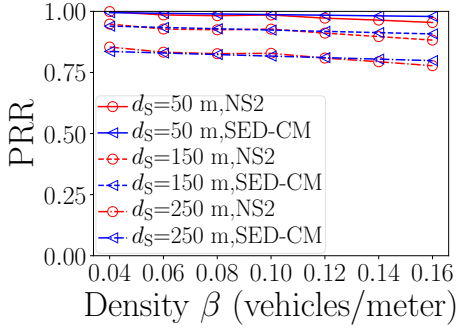
(a) PRPs



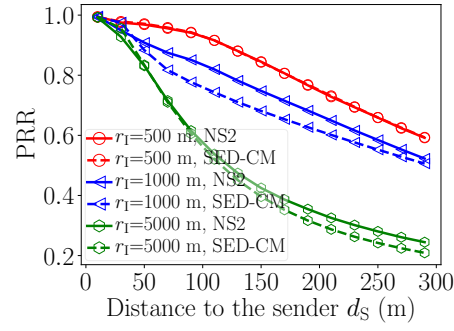
(a) PRPs



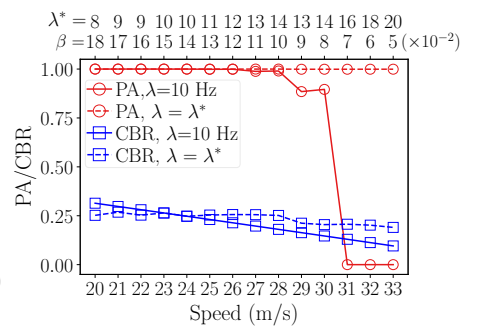
(a) The impact of speed of vehicle on the performance



(b) PRRs



(b) PRRs



(b) Comparisons between fixed beacon rate and optimal beacon rate

Fig. 17: Comparisons between the SED-CM model and NS2, 1D scenario, changing density

Fig. 18: Comparisons between the SED-CM model and NS2, Intersection scenario, changing  $r_1$

Fig. 19: Changing speed of vehicle in the 1D scenario

range 1000 m is regarded as the medium level interference range. Results show that the simulation yields better reliability than the model. Because in the NS2 simulation, the sensing power threshold is the average power at the receiving distance of 500 m. However, the detected power equals the sum of powers received from all the other transmitters. In this way, the sensing range of nodes in NS2 simulation is greater than 500 m, resulting in reducing the spatial reuse [50]. However, the sensing range is set to 500 m in the theoretical model. So that the results of NS2 simulation are better than the model. Moreover, Fig. 17 gives the PRPs and PRRs comparison between NS2 and the SED-CM model at changing densities when the maximum interference range is 500 m and the receiving distance  $d_s$  equals 50 m, 150 m, and 250 m, respectively. The densities is from 0.04 vehicles/meter to 0.16 vehicles/meter at an interval of 0.02 vehicles/meter. The results show that the results of the model are consistent with the results of NS2 simulation at different densities.

### B. Effect of the hidden terminal

We calculate the PRP only considering the impact of hidden terminal denoted by  $PRP_H$ , and  $PRP_H = PRP_{ht}^{E1} \times PRP_{ht}^{E2}$ .  $PRP_{ht}^{E1}$  and  $PRP_{ht}^{E2}$  in 1D scenario are shown (12) and (15), respectively. Fig. 16 shows  $PRP_H$  with different beacon rate  $\lambda$  and different sensing range  $r_E$ . The density is 0.1 vehicle/meter, the maximum interference range is 5000 m, the receiving distance is 130 m. The beacon rate  $\lambda \in [2, 30]$  Hz,

and the sensing range  $r_E \in [300, 800]$  m. It can be seen that the greater the beacon rate, the smaller  $PRP_H$  since the more opportunities for the hidden terminal to send. Moreover, the increased sensing range reduces the transmission opportunities of hidden terminals, thus increasing the  $PRP_H$ . In this way, we can reduce the interference caused by the hidden terminal by decreasing  $\lambda$  or increasing  $r_E$  individually or jointly. (8) shows that the sensing range is related to the ratio of the transmit power and the sensing threshold. It is simple to reduce the sensing threshold alone to increase the sensing range. However, it is complicated to increase the sensing range by increasing the transmission power because the data rate will increase, requiring a larger SINR threshold. The algorithms based on heuristics are expected to find the best parameters that meet requirements.

### C. PRPs and PRRs in the intersection scenario

Fig. 18 gives the PRPs and PRRs with the receiving distance at an intersection scenario. The length of each crossing road is 10000 m. The density on both the X-axis and Y-axis is 0.1 vehicles/meter. The results in Fig. 18 show similar behaviors as the results of 1D in Fig. 15. In this way, the same analysis for 1D is applicable to the intersection scenario. In the medium level interference range, the errors between the SED-CM model and NS2 in the intersection scenario seem larger than the 1D scenario. Since more nodes in the intersection simulation scenario increase the gap between the sensing range

in simulation and the theoretical sensing range, and increase the error of the results between the model and the simulation.

#### D. Effect of speed on the performance of system

We set the vehicle speed in [20, 32] m/s at the interval of 1 m/s. We map the speed of the vehicle to the density of the vehicle by (9), then calculate the performance metrics. Time headway  $T_{hw}$  is set 2 s. The tolerable time window  $T_a$  is calculated by (32). Fig. 19a shows PRP, PRR, and PA at different speeds with the packet generation interval of 0.1 s. The density corresponding to the given speed is shown at the top of the figure. We could find that PRPs and PRRs increase with the increase in speed. Because the greater the speed, the less the density, the fewer packets are lost due to collisions. However, the PAs decrease with the increase in speed. Because the greater the speed, the shorter the tolerance time window  $T_a$ . Moreover, the PAs decrease with increasing the number  $n$  of packets required by the safety application.

Then, for each speed of the vehicle, we compute the CBR and PA ( $n = 5$ ) of RCW with the packet generation rate  $\lambda$  from 5 Hz to 30 Hz at an interval of 1 Hz. Optimal beacon rate  $\lambda^*$  means that the PA is above the requirement 99.9%, and the CBR is minimal. Fig. 19b presents PA comparisons and CBR comparisons between fixed beacon rate  $\lambda = 10$  Hz and optimal beacon rate ( $\lambda = \lambda^*$ ) at different speed of vehicle. The densities and optimal packet generation rates are shown at the top of Fig. 19b. When  $\lambda = 10$  Hz, we could witness that PAs could meet the reliability requirement at the beginning when the speed is smaller than 28 m/s. However, the PA dropped sharply below the threshold due to the smaller tolerable time window when the speed is bigger than 28 m/s. The CBR presents a decreasing trend when increasing the speed of vehicle with the fixed beacon rate of 10 Hz. Because the density decreases with the increase in the speed of the vehicle. It is not difficult to find that the optimal packet generation rate  $\lambda^*$  increases with the increase in speed. With the optimal beacon rate, it is observed that the CBR keeps a value of about 0.25 over the various density of vehicles (speed of vehicle). In this way, when the vehicle is fast, the information is updated faster, more messages need to be sent for safety. Conversely, when the vehicle speed is slow, the information is updated slowly, and fewer message transmissions can ensure safety and relieve channel congestion.

### VIII. CONCLUSION

In the paper, we present an overview of the maximum interference range in VANETs. The maximum interference range relies on the minimum interference power that the device could perceive. We give the maximum interference range setting principle by obtaining the interference distance distribution in NS2. The greater the maximum interference range, the lower the reliability of VANET. Compared with the deterministic distance-based model, the SINR probability derivation-based model, and the SINR related effective distance-based model, the proposed SINR related Effective distance Constrained by the Maximum interference range-based (SED-CM) analytical model is proved to perform the

best evaluation when the interference range changes in the 1D and intersection scenarios. The larger error is caused when the maximum interference range is at a medium level because the sensing range in NS2 is larger than the theoretical sensing range. Moreover, our study found that the awareness probability of safety applications strongly relies on the quality of the channel and the tolerable time size. When the vehicle speed is greater, a faster beacon rate is expected.

The results presented in this paper suggest an important area of investigation is the impact of the maximum interference range variation on performance evaluation. Moreover, the maximum interference range should be incorporated into our existing communication framework for network planning and optimization. The inconsistency of the sensing range between the theoretical model and the NS2 simulation (equivalent to the actual device) has also been revealed to be an important factor affecting estimation accuracy. We will research the issue along with actual experiments in future work.

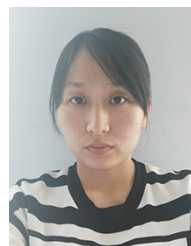
#### ACKNOWLEDGEMENT

We would like to thank the editors and anonymous reviewers for their helpful comments.

#### REFERENCES

- [1] O. Andrisano, R. Verdone, and M. Nakagawa, "Intelligent transportation systems: the role of third generation mobile radio networks," *IEEE Commun. Mag.*, vol. 38, no. 9, pp. 144–151, Sept. 2000.
- [2] X. Ma and K. S. Trivedi, "SINR-Based Analysis of IEEE 802.11p/bd Broadcast VANETs for Safety Services," *IEEE Trans. Netw. Service Manag.*, vol. 18, no. 3, pp. 2672–2686, Sept. 2021.
- [3] S. Zemouri, S. Djahel, and J. Murphy, "An altruistic prediction-based congestion control for strict beaconing requirements in urban vanets," *IEEE Trans. Syst., Man, Cybern. Syst.*, vol. 49, no. 12, pp. 2582–2597, Dec. 2019.
- [4] S. M. O. Gani, Y. P. Fallah, G. Bansal, and T. Shimizu, "A study of the effectiveness of message content, length, and rate control for improving map accuracy in automated driving systems," *IEEE Trans. Intell. Transport. Syst.*, vol. 20, no. 2, pp. 405–420, Feb. 2019.
- [5] A. Bazzi, B. M. Masini, A. Zanella, and I. Thibault, "On the Performance of IEEE 802.11p and LTE-V2V for the Cooperative Awareness of Connected Vehicles," *IEEE Trans. Veh. Technol.*, vol. 66, no. 11, pp. 10 419–10 432, Nov. 2017.
- [6] T.-S. Kim, H. Lim, and J. C. Hou, "Improving spatial reuse through tuning transmit power, carrier sense threshold, and data rate in multihop wireless networks," in *Proc. 12th MobiCom*, Los Angeles CA USA, 2006, pp. 366–377.
- [7] K. Xu, M. Gerla, and S. Bae, "How effective is the IEEE 802.11 RTS/CTS handshake in ad hoc networks," in *Proc. IEEE GLOBECOM*, vol. 1, Taipei, Taiwan, Nov. 2002, pp. 72–76.
- [8] R. Tandra and A. Sahai, "SNR Walls for Signal Detection," *IEEE J. Sel. Top. in Signal Process.*, vol. 2, no. 1, pp. 4–17, Feb. 2008.
- [9] X. Yin, X. Ma, and K. S. Trivedi, "An interacting stochastic models approach for the performance evaluation of DSRC vehicular safety communication," *IEEE Trans. Comput.*, vol. 62, no. 5, pp. 873–885, May 2013.
- [10] J. Zhao, Z. Li, Y. Wang, Z. Wu, X. Ma, and Y. Zhao, "An analytical framework for reliability evaluation of d-dimensional IEEE 802.11 broadcast wireless networks," *Wirel. Netw.*, vol. 26, pp. 3373–3394, Feb. 2020.
- [11] M. Ni, J. Pan, L. Cai, J. Yu, H. Wu, and Z. Zhong, "Interference-based capacity analysis for vehicular ad hoc networks," *IEEE Commun. Lett.*, vol. 19, no. 4, pp. 621–624, Apr. 2015.
- [12] J. Zhao, Y. Wang, H. Lu, Z. Li, and X. Ma, "Interference-based QoS and Capacity analysis of VANETs for Safety Applications," *IEEE Trans. Veh. Technol.*, vol. 70, no. 3, pp. 2448–2464, Mar. 2021.
- [13] Z. Tong, H. Lu, M. Haenggi, and C. Poellabauer, "A stochastic geometry approach to the modeling of DSRC for vehicular safety communication," *IEEE Trans. Intell. Transport. Syst.*, vol. 17, no. 5, pp. 1448–1458, May 2016.

- [14] X. Ma, J. Zhao, Y. Wang, T. Zhang, and Z. Li, "A New Approach to SINR-Based Reliability Analysis of IEEE 802.11 Broadcast Ad Hoc Networks," *IEEE Commun. Lett.*, vol. 25, no. 2, pp. 651–655, Feb. 2021.
- [15] "Receiver sensitivity and noise". Accessed: Feb. 16, 2022. [Online]. Available: [http://ftp1.digi.com/support/images/Whitepaper-Receiver-sensitivity-and-blocking.pdf%20\(48.05KB\).pdf](http://ftp1.digi.com/support/images/Whitepaper-Receiver-sensitivity-and-blocking.pdf%20(48.05KB).pdf)
- [16] Marbella, "Propagation model and interference range calculation for inductive systems 10 khz - 30 mhz," European Radiocommunications Committee (ERC), Tech. Rep., Feb. 1999.
- [17] G. Bansal, J. B. Kenney, and A. Weinfeld, "Cross-Validation of DSRC Radio Testbed and NS-2 Simulation Platform for Vehicular Safety Communications," in *Proc. IEEE VTC Fall*, San Francisco, CA, USA, Sept. 2011, pp. 1–5.
- [18] H. P. Luong, M. Panda, H. L. Vu, and B. Q. Vo, "Beacon rate optimization for vehicular safety applications in highway scenarios," *IEEE Trans. Veh. Technol.*, vol. 67, no. 1, pp. 524–536, Jan. 2018.
- [19] M. van Eenennaam, W. K. Wolterink, G. Karagiannis, and G. Heijenk, "Exploring the solution space of beaconing in vanets," in *Proc. IEEE VNC*, Tokyo, Japan, Oct. 2009, pp. 1–8.
- [20] M. I. Hassan, H. L. Vu, and T. Sakurai, "Performance analysis of the IEEE 802.11 MAC protocol for DSRC safety applications," *IEEE Trans. Veh. Technol.*, vol. 60, no. 8, pp. 3882–3896, Oct. 2011.
- [21] K. A. Hafeez, L. Zhao, B. Ma, and J. W. Mark, "Performance analysis and enhancement of the DSRC for VANET's safety applications," *IEEE Trans. Veh. Technol.*, vol. 62, no. 7, pp. 3069–3083, Sept. 2013.
- [22] Y. Yao, L. Rao, and X. Liu, "Performance and reliability analysis of IEEE 802.11p safety communication in a highway environment," *IEEE Trans. Veh. Technol.*, vol. 62, no. 9, pp. 4198–4212, Nov. 2013.
- [23] J. Zhao, Z. Wu, Y. Wang, and X. Ma, "Adaptive optimization of qos constraint transmission capacity of vanet," *Veh. Commun.*, vol. 17, pp. 1–9, Jun. 2019.
- [24] X. Ma, H. Lu, J. Zhao, Y. Wang, J. Li, and M. Ni, "Comments on "interference-based capacity analysis of vehicular ad hoc networks"," *IEEE Commun. Lett.*, vol. 21, no. 10, pp. 2322–2325, Oct. 2017.
- [25] H. ElSawy, A. Sultan-Salem, M.-S. Alouini, and M. Z. Win, "Modeling and analysis of cellular networks using stochastic geometry: A tutorial," *IEEE Commun. Surv. & Tutor.*, vol. 19, no. 1, pp. 167–203, Firstquarter 2017.
- [26] V. V. Chetlur and H. S. Dhillon, "Coverage and Rate Analysis of Downlink Cellular Vehicle-to-Everything (C-V2X) Communication," *IEEE Trans. Wirel. Commun.*, vol. 19, no. 3, pp. 1738–1753, Mar. 2020.
- [27] V. V. Chetlur and H. S. Dhillon, "Poisson line cox process: Asymptotic characterization and performance analysis of vehicular networks," in *Proc. IEEE GLOBECOM*, Waikoloa, HI, USA, Dec. 2019, pp. 1–6.
- [28] M. N. Sial, Y. Deng, J. Ahmed, A. Nallanathan, and M. Dohler, "Stochastic geometry modeling of cellular v2x communication over shared channels," *IEEE Trans. Veh. Technol.*, vol. 68, no. 12, pp. 11 873–11 887, Oct. 2019.
- [29] C. Campolo, A. Molinaro, A. O. Berthet, and A. Vinel, "On latency and reliability of road hazard warnings over the cellular v2x sidelink interface," *IEEE Commun. Lett.*, vol. 23, no. 11, pp. 2135–2138, Jul. 2019.
- [30] S. Lv, W. Zhuang, X. Wang, C. Liu, X. Hu, Y. Sun, and X. Zhou, "A performance study of CSMA in wireless networks with successive interference cancellation," in *Proc. IEEE Int. Conf. Commun. (ICC)*, Ottawa, ON, Canada, Jun. 2012, pp. 466–471.
- [31] Y. Yao, X. Chen, L. Rao, X. Liu, and X. Zhou, "LORA: Loss differentiation rate adaptation scheme for vehicle-to-vehicle safety communications," *IEEE Trans. Veh. Technol.*, vol. 66, no. 3, pp. 2499–2512, Mar. 2017.
- [32] W. Li, J. Wu, X. Ma, and Z. Zhang, "On reliability requirement for BSM broadcast for safety applications in DSRC system," in *Proc. IEEE Intell. Veh. Sym.*, Dearborn, MI, USA, Jun. 2014, pp. 946–950.
- [33] H. J. F. Qiu, I. W.-H. Ho, C. K. Tse, and Y. Xie, "A Methodology for Studying 802.11p VANET Broadcasting Performance With Practical Vehicle Distribution," *IEEE Trans. Veh. Technol.*, vol. 64, no. 10, pp. 4756–4769, Oct. 2015.
- [34] Y. Xie, I. W.-H. Ho, and E. R. Magsino, "The Modeling and Cross-Layer Optimization of 802.11p VANET Unicast," *IEEE Access*, vol. 6, pp. 171–186, Oct. 2018.
- [35] Q. Chen, F. Schmidt-Eisenlohr, D. Jiang, M. Torrent-Moreno, L. Delgrossi, and H. Hartenstein, "Overhaul of IEEE 802.11 modeling and simulation in ns-2," in *Proc. 10th ACM Symp. Modeling, Anal., Simul. Wirel. Mobile Syst.*, NY, United States, Oct. 2007, pp. 159–168.
- [36] X. Ma, S. Ding, C. R. Busse, and I. S. Esley, "Multi-layer QoS Analysis of IEEE 802.11bd Based VANET for Safety Applications," in *Proc. IEEE 18th Annu. CCNC*, Las Vegas, NV, USA, Jan. 2021, pp. 1–6.
- [37] E. Salahat and I. Abualhaol, "General BER analysis over Nakagami-m fading channels," in *Proc. 6th Joint IFIP WMNC*, Dubai, United Arab Emirates, April 2013, pp. 1–4.
- [38] J.-Y. Choi, H.-S. Jo, C. Mun, and J.-G. Yook, "Preamble-Based Adaptive Channel Estimation for IEEE 802.11p," *Sensors*, vol. 19, no. 13, July 2019.
- [39] M. Killat and H. Hartenstein, "An empirical model for probability of packet reception in vehicular ad hoc networks," *EURASIP J. Wirel. Commun. Netw.*, no. 721301, pp. 1–12, Mar. 2009.
- [40] T. S. Rappaport, *Wireless communications: principles and practice*, Second edition. prentice hall PTR New Jersey, 1996.
- [41] "Greenshield's Model". Accessed: Feb. 16, 2022. [Online]. Available: [https://www.webpages.uidaho.edu/niatt\\_labmanual/chapters/trafficflowtheory/theoryandconcepts/GreenshieldsModel.htm](https://www.webpages.uidaho.edu/niatt_labmanual/chapters/trafficflowtheory/theoryandconcepts/GreenshieldsModel.htm)
- [42] A. Iyer, C. Rosenberg, and A. Karnik, "What is the right model for wireless channel interference?" *IEEE Trans. Wirel. Commun.*, vol. 8, no. 5, pp. 2662–2671, May 2009.
- [43] J. Li, Y. Zhang, Z. Jing, X. Ma, and Y. Wang, "NS-2 Simulation of VANET for Safety Applications: Issues and Solutions," in *Proc. 8th Int. Conf. Comput. Model. Simul.*, Canberra Australia, Jan. 2017, pp. 67–72.
- [44] "2019 volkswagen e-golf se-specifications and price". Accessed: Feb. 16, 2022. [Online]. Available: <https://www.evspecifications.com/en/model/e1d178>
- [45] "Speeds and braking distances". Accessed: Feb. 16, 2022. [Online]. Available: <https://web.archive.org/web/20120622045505/http://www.unfallaufnahme.info/uebersichten-listen-und-tabellen/geschwindigkeiten-und-bremswege/index.html>
- [46] N. Kudarauskas, "Analysis of emergency braking of a vehicle," *Transport*, vol. 22, no. 3, pp. 154–159, Oct. 2007.
- [47] M. Taieb-Maimon and D. Shinar, "Minimum and comfortable driving headways: Reality versus perception," *Human factors*, vol. 43, no. 1, pp. 159–172, Mar. 2001.
- [48] T. Ayres, L. Li, D. Schleunig, and D. Young, "Preferred time-headway of highway drivers," in *Proc. IEEE Intell. Transport. Syst.(Cat. No. 01TH8585)*, Oakland, CA, USA, Aug. 2001, pp. 826–829.
- [49] K. Vogel, "A comparison of headway and time to collision as safety indicators," *Accident analysis & prevention*, vol. 35, no. 3, pp. 427–433, May 2003.
- [50] L. Fu, S. C. Liew, and J. Huang, "Effective Carrier Sensing in CSMA Networks under Cumulative Interference," *IEEE Trans. Mob. Comput.*, vol. 12, no. 4, pp. 748–760, April 2013.



**Zhijuan Li** received the M.S. degree at the School of Computer Science and Technology, Harbin Engineering University, Harbin, China, in 2013. From 2013 to 2016, she was a software engineer with Harbin Yuguang Virtual Network Technology Co., Ltd, China. She is currently working toward the Ph.D. degree with the School of Computer Science and Technology, Harbin Engineering University. Her research interests include vehicular ad hoc network and edge computing.



**Yanbin Wang** received the Ph.D. degree from the Industrial Engineering Department, Harbin Institute of Technology of China, in 2006. In 2010, he was a research associate with the Department of Electrical and Computer Engineering, Duke University, Durham, North Carolina. He is currently an associate professor in the Industrial Engineering Department, Harbin Institute of Technology of China. His research interests include vehicular ad hoc networks, quality management, scheduling, and optimization.



**Jing Zhao** received the Ph.D. degree in computer science and technology from the Harbin Institute of Technology of China in 2006. In 2010, she was with the Department of Electrical and Computer Engineering, Duke University, Durham, North Carolina, working as a postdoctoral researcher under supervision of Dr. Kishor Trivedi. She is currently a professor at the School of Software Technology, Dalian University of Technology, China. Her research interests include physical layer and MAC layer of vehicular ad hoc networks, reliability engineering, and network optimization.